Two-Neutron Correlations in the Photofission of Actinides

phd Thesis

Jeffrey S. Burggraf

January 19, 2018

Advisors: Prof. Dr. D. S. Dale

Department of Physics, Idaho State University

Abstract

Past study of fission reactions has established that fission neutrons are predominantly emitted by the fully accelerated fission fragments, as opposed to being emitted during scission. The velocities of the two fully accelerated fission fragments is of similar magnitude to the velocities of the fission neutrons as they are emitted in the fragment's rest frame. Thus, the motion of the fragments has a large effect on the kinematics of fission neutrons. This can be seen in the opening angle distributions of correlated neutron pairs from individual fission events. This effect has been measured multiple times for the spontaneous fission of ^{252}Cf and the thermal induced fission of ^{235}U with relatively good agreement. A primary motivation for this work is that to date there have been no reported measurements of this type with photofission. A project has been completed at the Idaho Accelerator Center to measure two-neutron correlations in photofission using bremsstrahlung photons produced via a low duty factor linear electron accelerator. The bremsstrahlung photons impinge upon an actinide target that is surrounded by a large neutron scintillation detector array capable of measuring particle position and time of flight, enabling the calculation of two-neutron opening angle and neutron energy. Correlated distributions in two-neutron opening angle, the angle between a neutron and the incident photon beam, and neutron energy are extracted from the data.

Contents

Chapter 1

Introduction

1.1 Physics of Nuclear Photofission

Photofission occurs during the de-excitation of a nucleus after the absorption of a photon. For photon energies between 6 and 25 MeV, this absorption occurs primarily through the giant dipole resonance (GDR). One distinct and useful aspect of photofission, particularly when compared to neutron-induced fission, is the simple set of selection rules for the transfer of angular momentum. In photofission, there is a relatively low transfer of angular momentum to the nucleus, and as a result photon absorption occurs primarily via E1 absorption and to a lesser extent E2 absorption. This restricts J^{π} values for even-even nuclei to 1^{+} and 1^{-}, and gives rise to anisotropies in the fission fragment angular distribution that are far more pronounced than they are for other types of fission [9]. For this reason, photofission is commonly used as a means to study sub-nuclear structures and the fundamentals of the fission process.

1.1.1 Neutrons from Photofission

Neutron emission can be classified into two categories: delayed and prompt. Delayed neutrons account for only $\sim 1\%$ of total neutron emission in actinide

photofission [3]. Delayed neutrons are not important to this study, since this measurement is insensitive to them. Prompt neutrons are defined as neutrons that are emitted either immediately after ($< 10^{-14}$ seconds), or during the scission of the nucleus, and account for the remaining $\sim 99\%$ of neutron emission [3]. Prompt neutron production is known to occur by means of two distinct mechanisms, the dominant of which is neutron emission from the fully accelerated fragments. The second mechanism, referred to as *early neutron* emission, is the emission of neutrons during either the scission of the nucleus or the acceleration of the fission fragments. Both cases are discussed below.

A large number of past studies have established that the majority of prompt fission neutrons (80%–98%) are emitted from the fully accelerated fragments [10], while the remaining 2%–20% percent are early neutrons. The nature of early neutrons has remained elusive ever since their first observation in 1962 by Bowman et al. [1]. Models of prompt neutron emission are based mainly on observations of neutron angular distributions relative to the fission axis–the axis along which the fragments travel in the center of momentum frame. Another observational input for prompt neutron modeling is the neutron-neutron (n-n) opening angle distribution of correlated neutron pairs. Because fission neutrons are predominantly emitted from the fully accelerated fragments, the distribution of n-n opening angles is highly reflective of the underlying fundamental fission kinematics.

There are, on average, about 2 or 3 neutrons released per fission. It has been shown that neutrons that are released from the fully accelerated fission fragments are evaporated isotropically in the fragment's rest frame, in which they are emitted at speeds comparable to that of the fragments themselves [14]. Thus, a significant portion of the kinetic energy of these neutrons comes from

the transnational motion of the fission fragments from which they are emitted. This leads to a characteristic distribution in the opening angles between pairs of neutrons, given that the neutrons came from the same fission event. To gain a qualitative understanding of the distribution, consider a pair of neutrons that are emitted from different fragments, which are moving in opposite directions. The boost that each neutron receives from the fragments will cause a tendency for the neutrons to travel in opposite directions. Because of this, the opening angle between them is more likely to be large, or close to 180°. Conversely, if two neutrons are emitted from the same fragment, they are both boosted in the same direction, which will tend to push them toward parallel trajectories. In this case, opening angles close to 0° are favored. The favoring of both small and large opening angles gives rise to a U-shaped distribution, where a minimum occurs near 90°.

A key feature of the two-neutron opening angle distribution is its dependence on neutron energy. As neutron energy increases, the characteristic U-shape of the opening angle distribution is expected to become stronger. In other words, there is a decrease in the rate of opening angles near the center of the distribution (at 90°) relative to the rates at 0° and 180°. This relationship is a direct consequence of the boost that the fission fragments provide to emitted neutrons. Fragments with the highest total kinetic energy give the largest boost to emitted neutrons. This, in turn, also intensifies the favoring of opening angles near 0° and 180°.

Scission neutrons

Scission neutrons are neutrons that are emitted before the rupture of the nucleus. The time between rupture and the emission of prompt neutrons is on

the order of 10^{-14} seconds, so timing cannot be used to distinguish prompt from scission neutrons. The existence of scission neutrons was first postulated by [1] in 1962, in order to explain a discrepancy between a neutron emission model, which was accepted at the time, and their measured angular distribution of prompt neutrons from the spontaneous fission of ^{252}Cf. By measuring the velocities of both fission fragments and a neutron–in 3-fold coincidence– the authors of [1] concluded that there must exist a small portion (10-15%) of emitted neutrons, dubbed scission neutrons, that are emitted isotropically in the lab frame before before scission. In the mid-late 1980s, this experiment was repeated by [15] and [2], who found that the number of scission neutrons is below 5% and 10%, respectively. In 2000, the authors of [7] claimed to have found errors in [1, 2], and [15], and that all three results reach an agreement of a 10% scission component after corrections for energy-resolution, timing, and neutron scattering from objects nearby the fission source. Most recently, [16] developed a "three-component" neutron emission model that accurately predicts the measured spectrum of gamma and neutron emission from ^{252}Cf. This model suggested a scission neutron component of $<$2%.

Scission neutrons are thought to be emitted isotropically in the lab frame, and so they have the effect of flattening out the "U"-shaped opening angle distribution. Because of this connection between neutron opening angle distributions and scission neutrons, opening angle measurements add to the growing breadth of nuclear data that is needed to shed light on the elusive scission neutrons, the understanding of which remains an open problem in nuclear physics.

1.2 Previous work

The first measurement of angular correlation among coincident neutrons from fission was performed by Debenedetti et al. [4] in 1948 using neutrons from the neutron induced fission of ^{235}U. It was already known at the time that fission neutrons are preferentially emitted in the same direction as the fission fragments. Because of this, in reference [4] it was hypothesised that there are measurable correlations between fission neutrons. This hypothesis was confirmed when they found that neutrons tend to be emitted preferentially at large opening angles. The next measurement of this type was performed nearly 30 years later by Pringle and Brooks in 1975 [13], in which neutrons emitted from the spontaneous fission (SF) of ^{252}Cf were found to have high coincidence rates at small opening angles near 0°, and at large opening angles near 180°. In order to remove the effects of detector geometry and efficiencies, reference [13] divided a correlated opening angle distribution by an uncorrelated opening angle distribution, which is similar to a technique used in this work. To date, numerous measurements of n-n angular correlation using ^{252}Cf have been performed (see works [13, 5, 12]). This makes ^{252}Cf a good benchmark for n-n angular correlation measurements. Other correlated n-n measurements have been performed using induced thermal induced fission of ^{235}U, ^{233}U, and ^{239}Pu [17]. This study is the first to report this type of measurement using neutrons from photofission.

Chapter 2

Methods

2.1 Experimental Apparatus

The experiment was carried out at the Idaho Accelerator Center, using their short pulsed linear accelerator. The accelerator is a radio frequency accelerator operating at the L–band frequency of 1300 MHz. It is capable of pulse widths ranging from 50 ps to 2 μs with a maximum energy of 44 MeV.

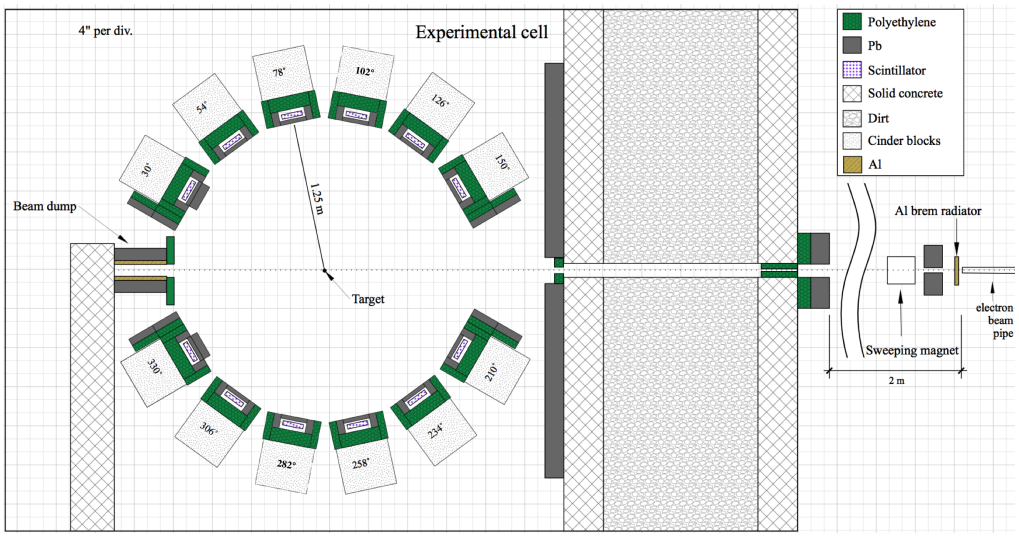

Figure 2.1: To-scale top down schematic of the entire experimental setup. The detectors supporting structures are each labeled with a degree value. The degree corresponds to the angle of the detector from the direction of the beam. For a better perspective of the scintillation cells alone, see 2.2

2.1.1 Detectors

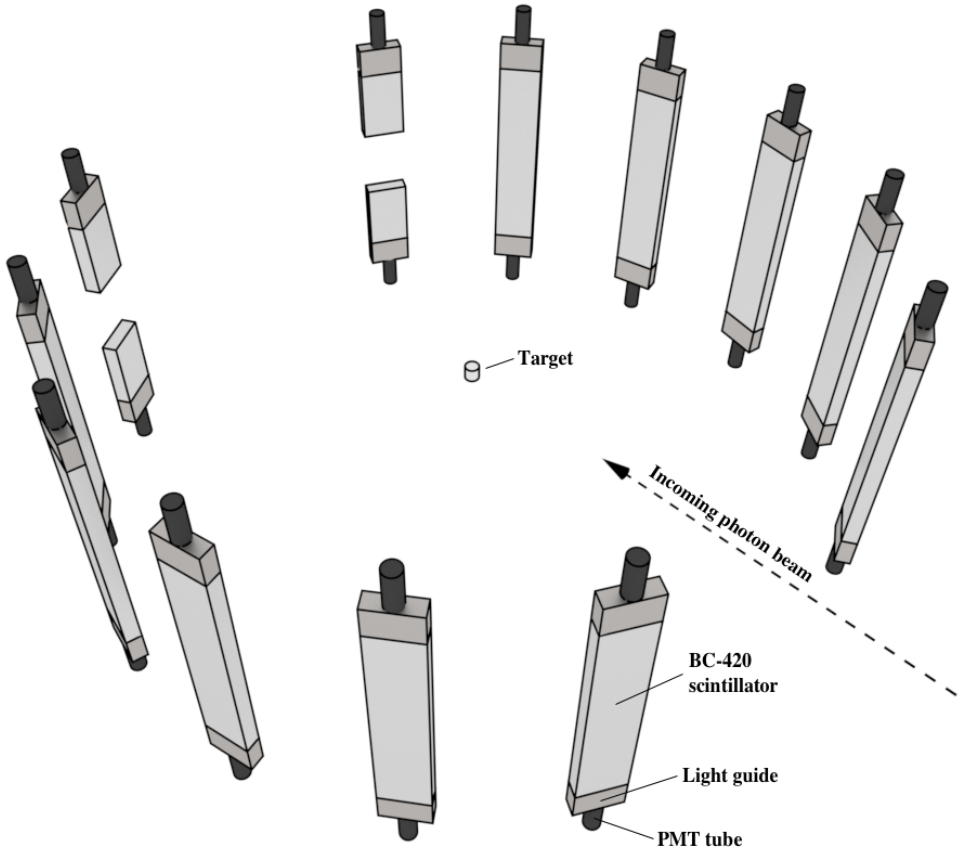

Figure 2.2: 3D-rendering of the bare scintillation cells showing how the detectors are positioned in space. Each detector is fully enclosed in a shielding structure, which is not shown in this depiction.

The neutron detector array consists of fourteen cells made from Polyvinyl Toluene, a type of organic plastic scintillator, acquired from the Transportation Security Administration (TSA) as surplus. The scintillation cells were arranged in a ring around the target (see figure 2.2). Each scintillator is instrumented with two Hamamatsu 580-17 photomultiplier (PMT) tubes, one fixed on each end. A 10 cm block of a non-scintillating material was fixed between each PMT and scintillator. This backs the PMTs off from the scintillator so that scintillation light produced near a corner of a scintillator has a line of sight to the PMT

nearest to that corner. Micro imperfections on the surface of the scintillation cells were reduced through polishing in order to increases the chance that scintillation light remains in the cell due to total internal reflection. The cells were then wrapped in reflective Tyvek in order to further facilitate the detection of scintillation light.

Two different detector designs had to be used in order to address a high rate of gammas on the detectors located furthest downstream of the beam. Ten of the fourteen detectors did not have this problem, and have dimensions of 76.2X15.2X3.8 cm^3. The remaining four had their dimensions reduced to 25.4X15.2X3.8 in order to address particularly rates of gamma detection, which are caused by the scattering of photons from the target. This scattering of photons creates a cone of gammas that engulfs forward facing detectors, leading to very high levels of dead-time and an effective neutron efficiency of zero. To counter this, the two downstream most detectors, at ± 30 degrees from the beam line, were reduced to 1/3 the size of the rest of the detectors and instrumented with only a single PMT . Prior to this modification, the gamma detection rate was nearly 1.0 per pulse in each. After the modification, the gamma detection rate fell to 0.5 gammas per pulse, which lead to a net increase in the effective neutron detection efficiency.

The location of a particle hit along the detector's 30 inch length is determined by the timing difference between signals in the top and bottom PMT . This method uses the fact that the scintillation light travels at a constant speed through the cell. This technique is not possible for the four the downstream detectors at $\pm 30^\circ$, since these have only a single PMT. For these detectors, particle position is assumed to be at the middle of the cell. For further detail on particle position reconstruction, see section 2.2.2.

2.1.2 Data Acquisition

A data acquisition system based on NIM/VME standard was used. A wiring diagram is shown in figure 2.3. The PMTs are supplied voltages ranging from 1300 to 1500 V by a Locroy 1458 high voltage mainframe. The analogue signals from the PMTs are fed into a leading edge discriminator with input thresholds ranging from 30 mV to 50 mV . The logic signals from the discriminator are then converted to ECL logic and fed into a CAEN model V1290A TDC . A gun signal from the accelerator provided the "start" signal for each pulse. On the software side, the acquisition of data from the TDC, along with the conversion of the data into usable formats, was carried out using the CODA software package developed by Jefferson Lab.

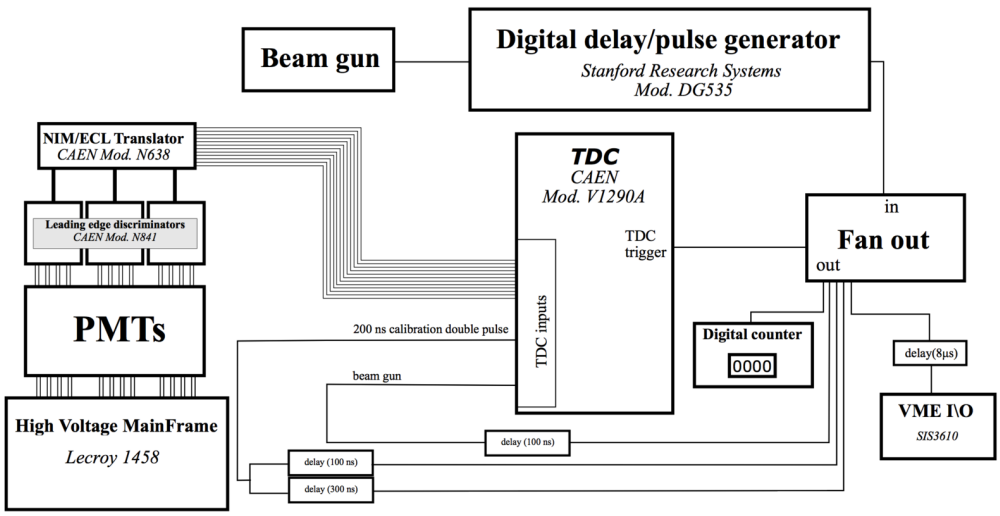

Figure 2.3: Wiring diagram of the entire electronics setup.

2.2 Experimental Methods

2.2.1 Photon Beam

A bremsstrahlung photon beam is produced passing 10.5 MeV electrons through a 1″ thick slab of aluminum. Aluminum was chosen as the radiator because it has a neutron knockout threshold above the energy of the electron beam. This ensured that the bremsstrahlung radiator would not be a source of fast neutrons which would have the potential to make their way into the experimental cell and cause false neutron events. Downstream from the bremsstrahlung radiator, a sweeping magnet removes excess electrons from the photon beam (see Figure 2.1). After the sweeping magnet, the beam travels through a series of polyethylene and lead collimators. Figure 2.4 shows the energy distribution of photons that reach the target according to MCNP simulation that included the creation and collimation of the bremsstrahlung photons.

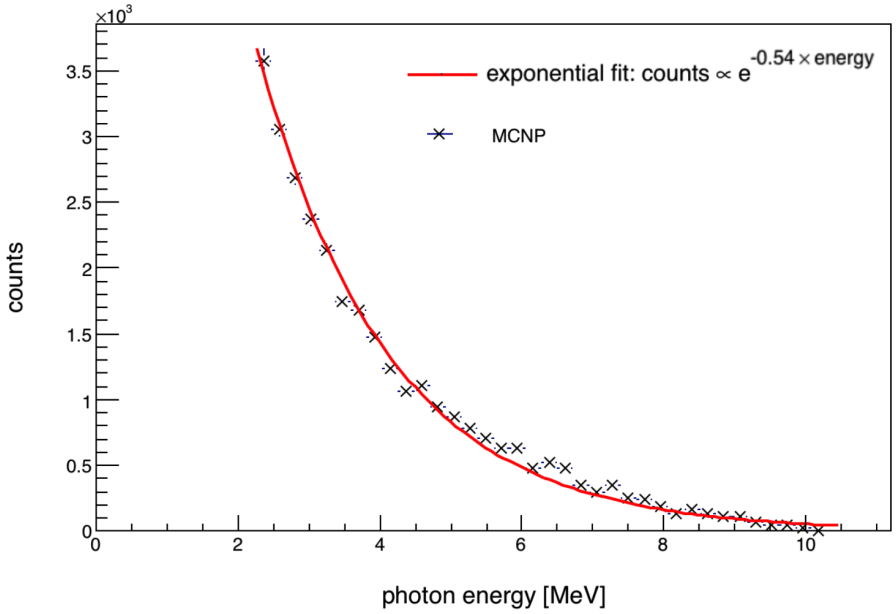

Figure 2.4: MCNP simulation of the energy distribution of the photons that reach the target. The points are from the simulation. The line is an exponential fit of the form Ae^{-bx}.

The reason for choosing a beam energy of 10.5 is that when attempting a measurement of prompt neutrons from photofission, an ambiguity can arise between neutrons from photofission and neutrons from (γ, xn) if x is greater than two. The two reactions have similar cross-sections within the GDR region, and there is significant overlap between the energy spectra of the neutrons. Because the current measurement is concerned only with observing two neutrons in coincidence, it suffices to set the Bremsstrahlung end-point below the target's $(\gamma, 2n)$ threshold, which is $\sim$12 MeV for ^{238}U. Setting the end-point below the $(\gamma, 2n)$ threshold does not eliminate the possibility of detecting two neutrons from two $(\gamma, 1n)$ reactions in a single pulse, which is referred to as an accidental coincidence. An *accidental* neutron coincidence occurs when two uncorrelated neutrons are detected in the same pulse. The rate of accidentals follow the poissonian distribution, setting them apart from correlated events, and as a result, accidentals can be subtracted from the data. The details and justifications for this procedure are discussed in section 2.3.2.

The electron beam pulse width was set to 3 ns and had a 1.1A peak current, with a repetition rate of 240 Hz. The 3 ns pulse width is not a large source of error in the measurements of neutron time of flight (ToF), since neutron events had a median TOF of $\approx$80 ns. ToF is the time taken for a particle to travel from the target to the face of a detector. The accelerator's current was set by requiring that there be, on average, fewer than one fission per pulse in order to diminish the number of accidentals.

2.2.2 Particle time of flight determination

ToF was used to distinguish between photons and neutrons, and to measure neutron energy. Each of the scintillators were equipped with two PMTs, one

fixed at each end of the scintillator, with the exception of those located farthest downstream at $\pm 30^{\circ}$ which each had a single PMT (see Figure 2.2). In order to diminish dead-time, the detectors at $\pm 30^{\circ}$ were segmented to create two independent detectors. See section 2.1.1 for a more detailed discussion about the detector design. ToF was determined by averaging the timing of signals from both PMTs of a given detector, then subtracting a constant calibration offset. The timing of events in the PMTs were always measured relative to a signal provided by the accelerator at the beginning of each pulse, referred to as the *beam gun*. The timing resolution of each PMT is 2ns [6].

Scintillation light that is detected by the PMTs has an effective index of refraction of ~ 3, which is greater than the actual value for that material. This difference is due to the multiple reflections of the scintillation photons from the optical boundaries of the detector which increased the time of the light collection. Consequently, there can be up to an 8 ns delay between when a particle scintillates in the detector and the scintillation light reaches a PMT. The effective index of refraction was found by measuring the time taken for scintillation light to travel the full length of the detector. The time of flight was calculated by taking the average between the times of signals in the top and bottom PMTs, and then subtracting a calibration offset. In taking the average, there is a reduction in the sensitivity of the result to the variation of propagation times as a function of the position at which the particle scintillated. This cannot be done in the detectors located at $\pm 30^{\circ}$, because they have only one PMT. However, since they are $1/3$ the length of the rest, scintillation light takes at most only 2.5 ns to propagate to the PMT, which is a tolerable amount of random error. See section 4 for a deeper discussion of experimental errors.

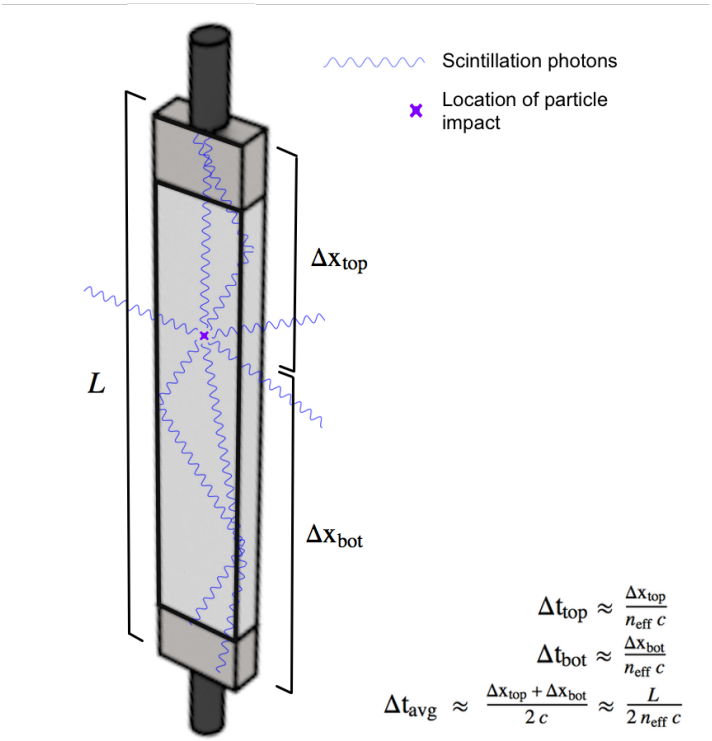

Figure 2.5: The average of times taken for scintillation light to travel from the point of its creation to each PMT has low variance. This average includes the time required for light to travel the full length of the detector, which is a constant for photons that travel exactly parallel to the length of the detector. Scintillation photons that travel parallel to the length of the detector are favored for detection by the PMTs because they reach the PMT first and experience less attenuation. Therefore, the distribution of Δt_{avg} is reflective of the ToF distribution of the particle's producing scintillation light.

The ToF of a particle obeys the following relationship:

$$\text{ToF}_i = t_i^0 + \Delta t_{\text{avg}}$$

where ToF_i is the ToF of a particle observed in detector i, t_i^0 is a constant timing offset, which is the same for every pulse, and Δt_{avg} is the average between the timing of signals in the top and bottom PMTs of a given scintillator. The reason for the subscript, i, is that the timing offset is different for each scintillator due to, for example, differences in the lengths of the PMT signal cables. Any

process that produces a timing delay that does not change from pulse to pulse contributes to t_i^0. Examples of this are:

- the time required for photons to travel from the bremsstrahlung radiator to the target
- the propagation of signals through the wires connecting the PMTs
- delays in the electronics
- the transit time in the PMTs.
- the time required for scintillation light to propagate from the point of creation to both PMTs.

The final example above is nearly constant only after the average between two PMTs is taken, Δt_{avg}, at which point this effect produces standard deviation of 3 ns in measured ToF. The time required for scintillation light to travel to a single PMT can vary from $\approx$1 ns for particles that scintillate near a PMT, to $\approx$10 ns for particles that scintillate at the opposing end of the scintillator. Variance in ToF measurements due to this is reduced by taking the average between the timing of signals from both PMTs of a scintillator. Δt_{avg} is $1/2$ times the sum of the two times, and this sum includes the time for light to travel to both PMTs, which is just the time for light to travel the total length of the detector. This value is a constant if the scintillation light travels parallel to the detector's length. This isn't always the case, however, so the effective velocity at which scintillation light travels lengthwise through the detector has non-zero variance which contributes to the uncertainty of ToF measurement. The setup favors the detection of scintillation photons that travel lengthwise through the scintillator, since these travel the shortest distance and therefore experience less attenuation. In taking the average between two PMTs, the

uncertainty in ToF is reduced by about a factor of three compared to using a single PMT.

The variance of the effective velocity of scintillation light was measured using a ^{60}Co source, which emits coincident photons. The ^{60}Co source is placed at five positions along the face of a lead shielded scintillator. At each position, a small hole is drilled through the lead to give the ^{60}Co source a line-of-sight to a well defined point on the scintillator. A high timing-resolution photon detector is placed next to the ^{60}Co source, hereafter referred to as the trigger. With the ^{60}Co source in place, coincident rate between the trigger and the scintillation detector increases by orders of magnitude compared to baseline. This increase is caused by two coincident photons reaching the trigger and the scintillation detector at the same time. With this setup, the time of at which the decay occurred is known from the high trigger, and thus so is the time of scintillation. This allows the study of the times taken for scintillation light to propagate through the scintillator. The times of signals from each PMT, taken relative to the trigger, are averaged. These results can be seen in figures 2.6 and 2.7.

The value of the constant offset for ToF calculation is determined by observing photons that scattered from the target. Comparing the timing spectra of a non-neutron producing target made from aluminum, to the spectra produced when no target is used reveals a prominent peak caused by the scattering of photons from the target. Aluminium does not produce photo-neutrons because the beams's Bremsstrahlung end-point is below Aluminium's (γ, n) threshold. Photons scattered from the target must travel between 125 cm to 130 cm to reach a face of a detector, depending on whether the photons reach the detector near the center or at the edge. It takes light 4.0 ns and 4.3 ns to travel 125

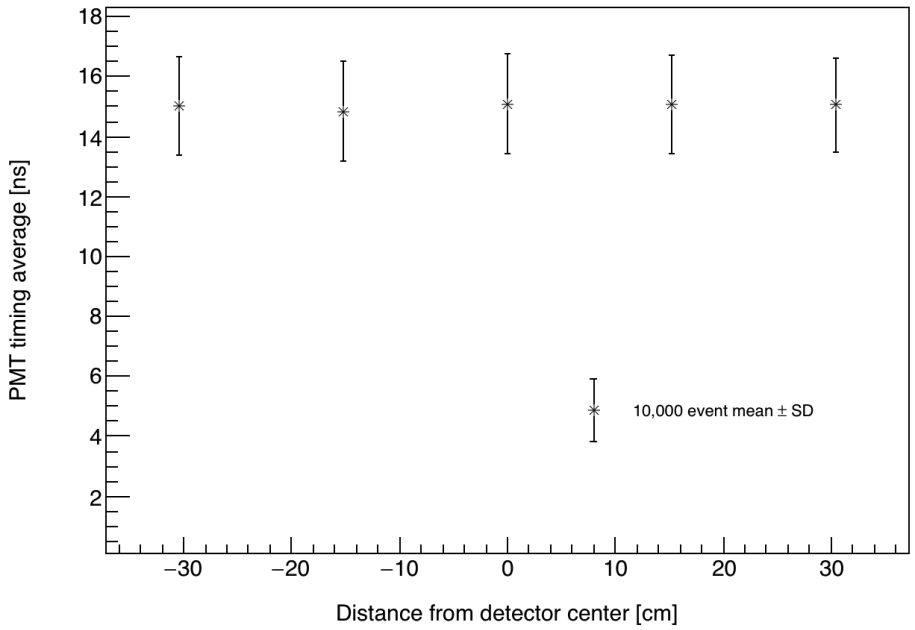

Figure 2.6: A ^{60}Co source, which emits coincident photons, is placed at five differnt positions along the face of a lead shielded scintillator. At each position, a small hole is drilled through the lead to give the ^{60}Co source a line-of-sight to a well-defined point on the scintillator. Then, a high timing resolution scintillation photon detector made from ATP plastic is placed close to the ^{60}Co source. When the ^{60}Co source decays, emitting two photons simultaneously, one photon is detected by the high timing-resolution detector serving as the "start" time, and the other scintillates in the detector being calibrated.

cm and 130 cm, respectively. The difference between these two times is negligible for these purposes, so the ToF of photons that scatter from the target is assumed to be 4 ns. With this assumption, the location of the photon peak in the timing spectra can be used to calculate the offset in each detector. See figure 2.8 for an illustration of this process.

2.2.3 Particle Position Reconstruction

Spacial resolution in the horizontal plane is determined by the physical dimensions of the detector. The geometric center of a detector is used for the position, in the horizontal plane, of a particle hit. The detector's dimensions in the horizontal plane are comparatively small at 3.8x15 cm^2, so in doing this,

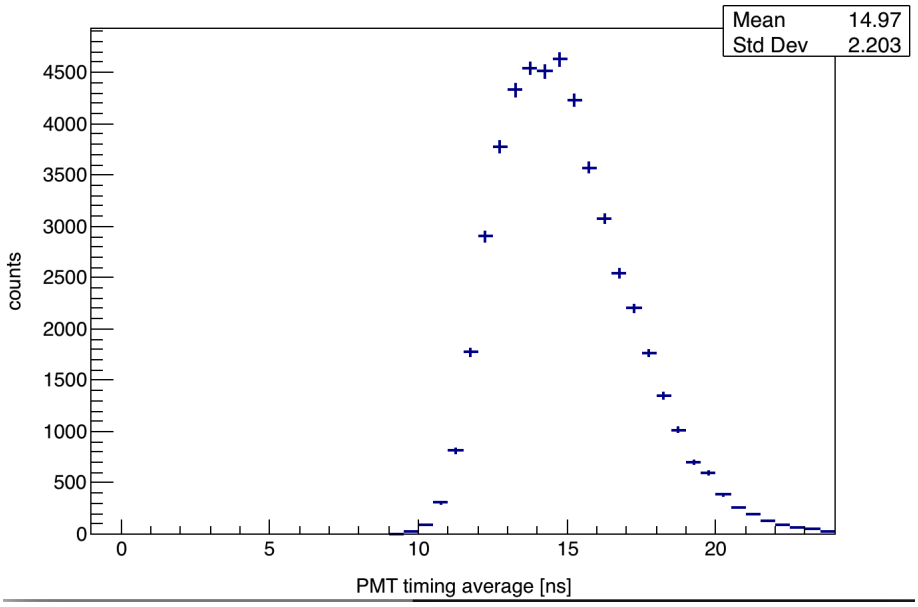

Figure 2.7: The sum of times in the top and bottom PMTs are reflective of the time taken from scintillation light to travel the full length of the scintillator. Taken during calibration with a ^{60}Co source. Ideally, the time taken for scintillation light to travel the length of the detector would be a constant, and the ToF resolution would be equal to the resolution of the PMTs at ≈ 1 ns. This is not the case, however, because scintillation light doesn't always take the shortest path to a PMT. The 3 ns standard deviation of this curve represents the uncertainty in the time at which a particle is detected. This plot is the result of projecting the data used in fig **??** onto the y-axis.

a positional uncertainty of ± 7.5 cm is introduced, which expressed in terms of an angle is $\pm 4^\circ$. The final results of this work use an opening angle bin width of 20°, so $\pm 4^\circ$ is not large enough be a cause for concern. The largest contributor to uncertainty in particle position is the position in the vertical direction, which is determined by the timing difference between signals in the top and bottom PMTs.

The determination of a particle's position in the vertical direction relies on the timing of coincident signals from both the PMTs of a detector. The timing difference obeys a linear relationship with respect to the location of the particle hit along the length of the detector. The z-coordinate will hereafter refer to a

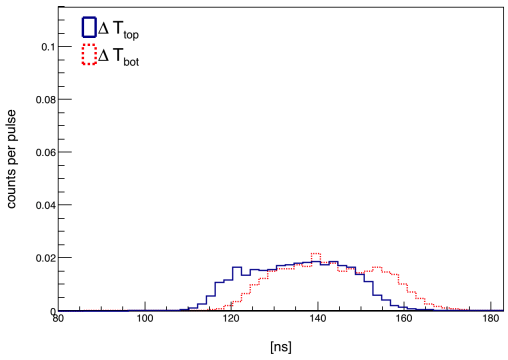

(a) ΔTs with no target in place.

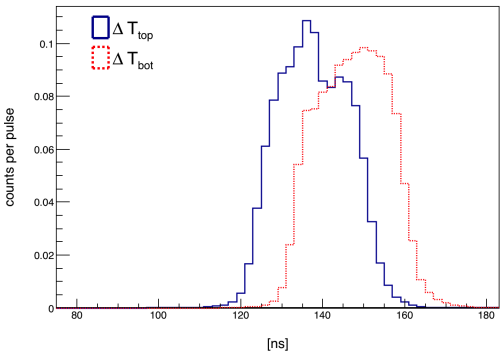

(b) ΔTs with Aluminum target.

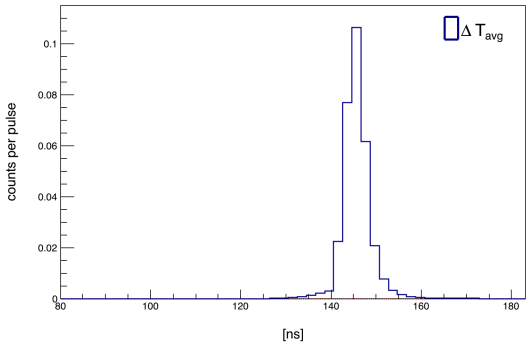

(c) Average of ΔT_{top} and Δt_{bot} with Aluminum target in place.

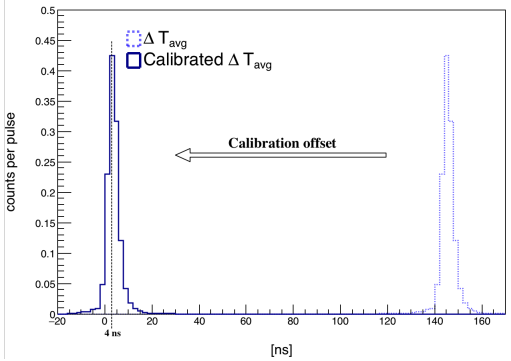

(d) Application of a calibration offset.

Figure 2.8: (a) ΔT spectra from both PMTs of a detector while no target is in place. (b) The introduction of a non-neutron producing target, made from aluminum, produces a prominent peak caused by the scattering of photons from the target. (c) Taking the average between the ΔTs of the top and bottom PMTs produces a sharper peak than in (b), since the sum of times from both PMTs is a reflection of the time required for light to travel the entire length of a detector, regardless of the location of the particle hit. The width of this peak if reflective of the uncertainty in time of flight measurements. (d) A calibration offset is applied so that the photons have the correct time of flight of 4 ns.

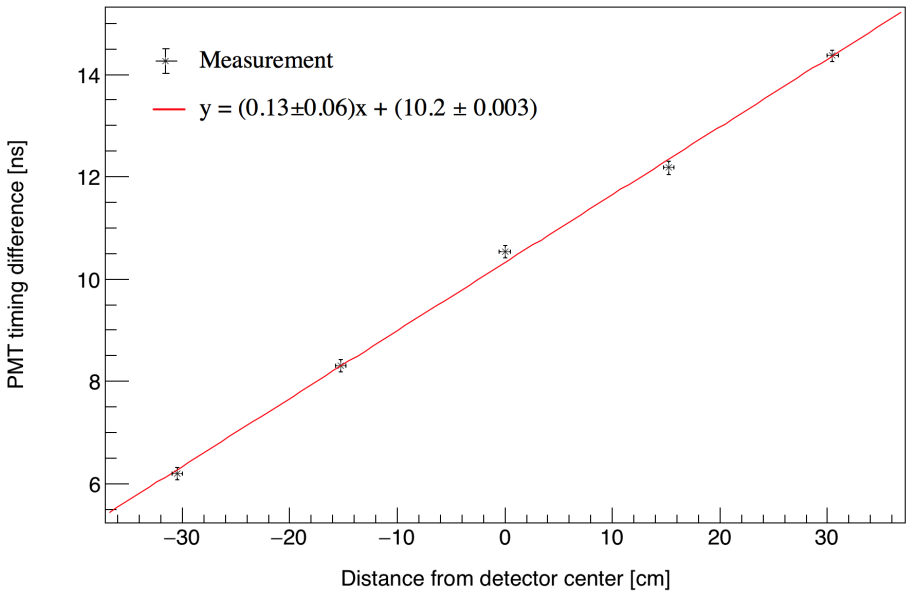

Figure 2.9: A collimated ^{60}Co source is used to produce events at five precise locations on the detector. The particle's position along the detector's length is shown to vary linearly with respect to the timing difference between events in the top and bottom PMTs of a detector.

particle's position along the vertical axis, where $z = 0$ corresponds to the geometric center of the detectors.

As discussed before, detected scintillation light tends to take fairly direct paths to the PMTs, experiencing few reflections off the boundary of the scintillation cell. As a result, the timing difference between signals in the top and bottom PMTs is proportional to the difference in path lengths that the scintillation light must travel to reach each PMT, which is in turn proportional to the z-coordinate of the particle hit. The exact linear relationship is determined through calibration by using collimated photons from a ^{60}Co source. Calibration is achieved by measuring the PMT top-bottom timing difference while the ^{60}Co source is fixed at five different locations along the detectors length. The setup for calibration was discussed in section 2.2.2. The result is shown in figure 2.9.

Detector Shielding

The detector's shielding was designed with the aim of reducing cross-talk, the detection of photons, and noise. The front face of the detectors, facing towards the target, were subject to the highest gammas flux due to the scatting of the beam from the target. The detection of a gamma renders a detector "dead" during the time at which subsequent fission neutrons from the same pulse reach the detector. Lead can mitigate this problem by attenuating gammas, but has the side effect of scattering neutrons. If a neutron scatters prior to being detected, the ToF calculation will be incorrect because the neutron traveled an unknown distance to the detector. The extent that neutron distances of travel are perturbed due to scattering from lead shielding was quantified using an MCNP . Accordingly, 1" of lead was placed along the front face of the detectors. This diminished gamma detection rates to reasonable levels and, according to the simulation, caused a negligible amount of neutron scattering. Because of particularly high gamma flux, an additional 2" of lead was placed at the sides of detectors adjacent to the beam, and along the front faces of the detectors farthest downstream at $\pm 30^{circ}$ from the beam line. Placing lead behind the detectors was avoided in consideration of an MCNP-POLIMI simulation, which indicated that lead placed here facilitates cross-talk. Because cross-talk events are in fact correlated, they cannot be removed in analysis by the subtraction of accidentals. For more information about cross-talk, see section 4.2.1.

2.2.4 Targets

A depleted uranium (DU) target with dimensions of 4x2x0.05 cm^3 was used as the primary target for the measurement of two-neutron correlations. DU received the majority of the allotted beam time because it is an even-even

Pictues of target

nucleus and as a consequence the fission fragments are emitted with a high degree of anisotropy [9].

It is desirable to have a target geometry with symmetry that is consistent with the cylindrical symmetry of the neutron detector array. To accomplish this, a thin rectangular target was rotated slowly about the vertical axis during data acquisition. In doing so, the measurement is reflective of the average of events which occurred while the target was at all orientations between 0 and 2π, thereby cylindrical symmetry is effectively preserved. This eliminates potential biases caused by the asymmetrical structure of the target.

2.2.5 Measurements with ^{252}Cf

Opening angle measurements were also performed on neutrons from the spontaneous fission (SF) of ^{252}Cf. There is good agreement among past measurements of the opening angle distribution of neutrons from the spontaneous fission of ^{252}Cf, and so such measurements serve as a means to validate the methods used in this study.

As opposed to the measurements of neutrons from photofission, there is no concern over the detection of accidental neutron pairs, because given the strength of the ^{252}Cf source, it is highly unlikely that two fissions occur during the acceptance time window of 150 ns. Another difference between the two measurements is the clean and sharp peak produced by fission photons from ^{252}Cf, compared to a relatively smeared peak produced by photons scattering from the target during measurements of photo-neutrons. In each measurement, the photon peak is used as a reference point for the calculation of neutron ToF. As a result the ^{252}Cf measurements have less error in ToF caused by the spreading of the photon peak used for reference. The same normalization technique is

used for both measurements, in which the correlated distribution is divided by the uncorrelated distribution of neutron pairs taken from different fissions.

The configuration for this was different than that for photofission measurements, as the photon beam can no longer be used for the timing of a "start" trigger. The trigger for ^{252}Cf consisted of two high timing-resolution scintillation photon detectors made from ATP plastic, where one is fixed below and the other above the source at a distance of 15 cm. Using a coincidence window of 4 ns, the timing start trigger required 2-fold coincidence between both the photon detectors. Aside from a different mechanism for a start trigger, the methods used for the measurement of two-neutron opening angle distributions in the SF of ^{252}Cf are equivalent to those used for photofission.

2.3 Data Analysis

2.3.1 Calculation of Angular Correlation

The efficiency and acceptance of the neutron detector array varies greatly over the range of opening angles from 0 to 2π (see figure 2.10(a)). This effect is due both to the detector array's non-spherical symmetry, and to varying efficiency as a function of particle position. Knowledge of the array's efficiency as a function of two-neutron opening angle is not needed, because angular correlation is determined by normalizing raw opening angle measurements to an equivalent distribution of uncorrelated neutrons, giving a result that is insensitive to detector efficiencies, while remaining sensitive to angular correlations. The effect of normalization is illustrated in figure 2.10. Figure 2.10(a) shows the unnormalized two-neutron opening angle distribution from the spontaneous fission of ^{252}Cf. The structure is reflective of the geometric acceptance and efficiencies

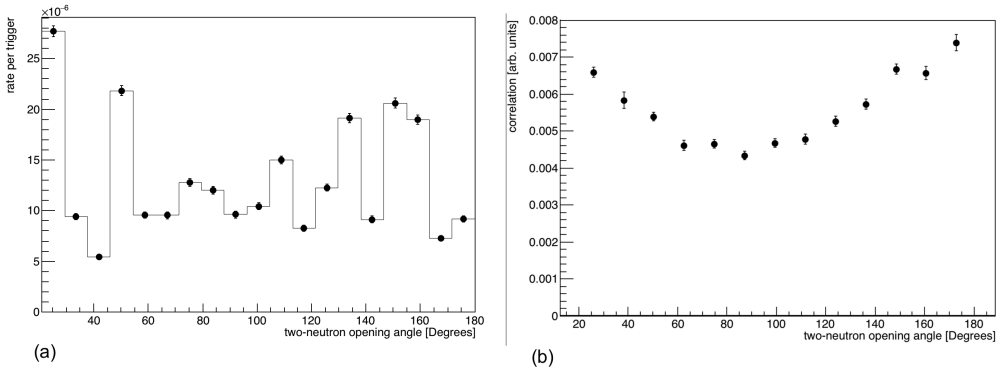

Figure 2.10: (a) Unnormalized two-neutron opening angle distribution from the spontaneous fission of ^{252}Cf (b) The distribution after normalizing to the distribution of uncorrelated two-neutron events.

of the neutron detector array. Fig 2.10(b) shows the normalized distribution. Normalization is achieved by dividing the raw opening angle distribution by the opening angle distribution formed by uncorrelated two-neutron events in which each neutron is taken from a different fission. When the beam is in use, neutron events from different pulses are used instead. Such neutron pairs will hereafter be referred to as different pulse (DP) pairs.

The neutrons of a DP pair are uncorrelated because events in one pulse do not have casual influence on the events in another pulse. Detector efficiency and geometry influence same pulse (SP) events and DP events equally.Thus, barring two-neutron correlations and a scaling factor, the DP distribution is identical to the SP distribution. Each pair of pulses is chosen such that the two pulses occurred within less than a few 100 ms of each other. This ensures that both pulses are subject to the same experimental conditions, thereby lessening systematic effects from time varying factors such as high-voltage drift, varying beam current, and detector thresholds. As many pairs as needed can be readily selected until good counting statistics is achieved, because the only restriction for selecting pulse pairs is that they occurred around roughly the same time.

ToDo: further explain why this statement holds true

2.3.2 Subtraction of Accidentals

An accidental neutron coincidence is defined as a coincidence between two uncorrelated events in a single pulse. For example, a coincidence between a neutron from a (γ,1n) reaction and a neutron from photofission. Another example is a coincidence between two events that are part of the noise background. In both of these examples, the two events are considered accidentals because they have no causal influence on each another. A true neutron coincidence, or true for short, is defined here as any pair of correlated neutrons from the same pulse.

Accidentals are removed from the data by subtracting 1/2 times the equivalent distribution formed by the DP data. The factor of 1/2 arises from the Poissonian statistics that inherently govern all accidentals, whether the accidental events are composed of two neutrons, two photons, two noise events, or any combination thereof. An accidental is comprised of the occurrence of two independent events. Therefore, as per Poissonian statistics, the probability of measuring an accidental in a single pulse is given by:

ToDo: Explain why the use of Poissonian statistics is valid. Mention the fact that we only take the first hit

$$SP_{\mathrm{a}} = \frac{e^{-\lambda}\lambda^2}{2} \approx \frac{1}{2}\lambda^2$$

where SP_a is the accidental rate of single pulses, λ is the mean accidental rate of single pulses–an unknown value. In this study, the coincidence rates were around 5×10^{-5} events per pulse, so the approximation used above is correct to within 0.001% as the worst case scenario. Since the DP data is formed by observations of events from two different pulses, the DP accidental rate is

equal to the poissonian probability of observing exactly one event, squared:

$$DP_{\mathrm{a}} = (e^{-\lambda}\lambda)^2 \approx \lambda^2$$

where DP_{a} is the accidental rate of DP events. Therefore, the rate of detected accidentals in single pulses is $1/2$ times the rate at which accidentals occur in the different pulse data. The subtraction of accidentals was about a ten percent effect. A relatively low accidental rate was the intended outcome of setting the beam current low enough such that there is, on average, less that one fission per pulse.

Chapter 3

Results

Chapter 4

Discussion of Experimental Errors

All sources of error in this study can be classified into three groups: **1. Resolution of measurement**, a source of random error reflective of the precision of particle ToF and position measurements, **2. Counting error**, another a source of random error, and lastly, **3. Systematic errors**, the mitigation of which has motivated detector design and new methods for data analysis.

4.1 Random Errors

4.1.1 Resolution of measurement

The position of a detected particle is known to within a specified resolution, which translates into a resolution in the measurement of the opening angle between a pair of particles. A particle's reconstructed position along a detector lengthwise is achieved by using the timing difference between two PMTs, producing a result known to within ± 13 cm.Due to the detector's 15 cm width, there is also a positional uncertainty of ± 7.5 cm in the direction perpendicular to the detector's length. The amount of uncertainty in a two-neutron opening angle measurement is a function of the uncertainty in the positions of each neutron. This function is determined by the propagation of the positional uncertainties through the formula for the calculation of opening angle, which is

Use my plot on wiki of PMT diff with Co60 at the center. Use this to deduce the vertical position uncertainty.

given by

$$\theta_{nn} = \arccos\left(\frac{\vec{v_1} \cdot \vec{v_2}}{|\vec{v_1}||\vec{v_2}|}\right)$$

where $\vec{v_1} = (x_1, y_1, z_1)$ and $\vec{v_2} = (x_2, y_2, z_2)$ are the detected positions of the two neutrons. The propagation of error through this formula is achieved by evaluating the following expression

$$\begin{aligned}\Delta\theta_{nn} = \Bigg(&\left(\Delta x_1 \frac{\partial\theta}{\partial x_1}\right)^2 + \left(\Delta y_1 \frac{\partial\theta}{\partial y_1}\right)^2 + \left(\Delta z_1 \frac{\partial\theta}{\partial z_1}\right)^2 + \\ &+ \left(\Delta x_2 \frac{\partial\theta}{\partial x_2}\right)^2 + \left(\Delta y_2 \frac{\partial\theta}{\partial y_2}\right)^2 + \left(\Delta z_2 \frac{\partial\theta}{\partial z_2}\right)^2\Bigg)^{\frac{1}{2}}\end{aligned}$$

Mention what the deltas are in this big formula.

Then, by using a set of opening angle bins, the average is computed of the propagated uncertainties of the measurements in each bin. The result, seen in fig 4.1, can be interpreted as the opening angle resolution as a function of θ.

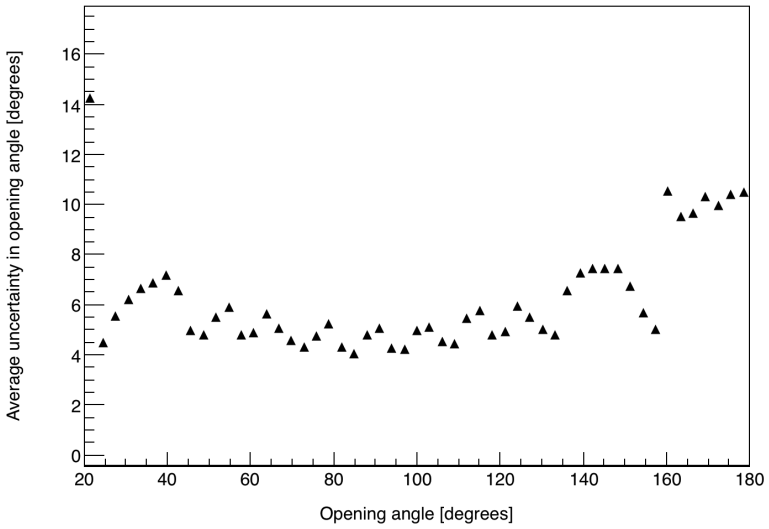

Figure 4.1: Uncertainties in opening angle as determined by the propagation of position uncertainties through the opening angle calculation. Because the uncertainty of a given opening angle measurement varies depending on which two detectors are involved, an average of the calculated uncertainties of measurements falling within each bin is taken. The y-axis can be viewed as a measure of the angular resolution in the sense that it represents the smallest angular difference that can be considered statistically significant.

4.1.2 Counting error

The standard deviation in the number of observed events is always assumed to be equal to $\sqrt{N}$, as per poissonian statistics, were N is the number of observed events. Opening angle measurements are separated into three different neutron energy ranges and then placed into bins 10 degrees wide. These groups each contain between 100 and 200 events, producing a relative error between 10 and 7 percent, respectively. The vertical error bars seen in the results are solely a reflection of such counting error.

4.2 Systematic errors

This study reports two-neutron opening angle distributions expressed as a ratio between a correlated distribution and an uncorrelated distribution in which the same set of neutron events are used to form both distributions. In doing so, the result is unaffected by the absolute neutron efficiencies and thresholds of each detector, drifting of the high voltage supplied to the PMTs, and the geometrical acceptance of the detector array as a function of opening angle. Furthermore, *accidental* two-neutron events, which lead to an over estimation of the isotropic component of the opening angular distribution, are subtracted from the data. *Accidental* two-neutron events are defined as the detection of two causally uncorrelated events in the same pulse if both events occur during the neutron ToF window. The subtraction of such events is possible under the assumption that the number of detected accidentals per pulse follows the poissonian distribution. See section 2.3 for a detailed discussion on how the subtraction is accomplished. The validity of this assumption can be tested with measurements taken while using D_2O as a target. All coincident neutrons observed from the photo-disintegration of deuterium are accidentals because

only one neutron is produced per disintegration. Figure 4.2a shows that a poissonian model gives a good fit to the distribution of the number of neurons detected in coincidence while using a D2O target. When observing neutrons from photofission, on the other hand, there is the inclusion of correlated neutrons, together with accidental neutrons caused by multiple fissions or (γ, n) reactions, so a poissonian model underestimates the rate of two-neutron coincidence. See fig 4.2.

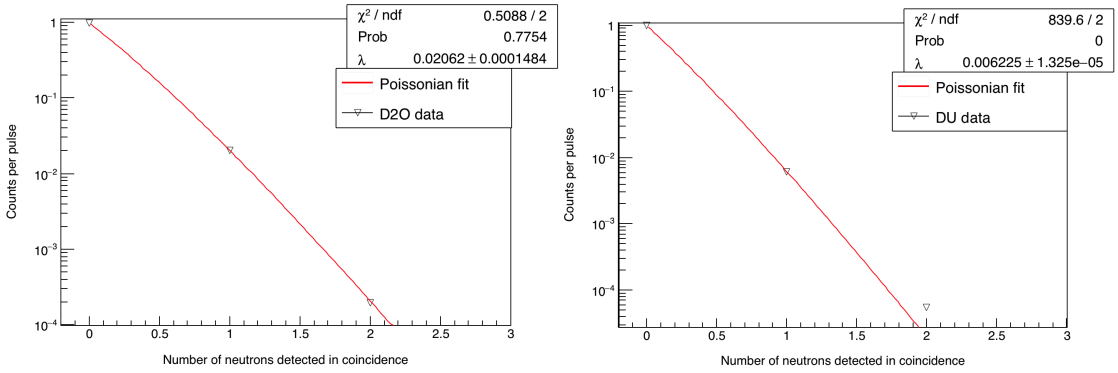

(a) D_2O target: prob near 1.0, good compatibility. (b) DU target: prob is 0, poor compatibility.

Figure 4.2: A D_2O target (left) produces only accidental neutrons, so a poissonian model is suitable. The p-value, denoted "prob" on the plot, is a metric for assessing the compatibility of the data to a given model, poissonian in this case. A p-value of 0.77 for the D_2O target indicates relatively good compatibility. On the other hand, when using DU as a target (right), the introduction of correlated neutrons causes the poissonian model to under estimate the double-coincidence rate. The assumption that the coincidence rates of accidental neutrons follow the poissonian distribution is used to subtract accidentals from the data, removing this source of systematic error.

4.2.1 Detector Cross-talk

Cross-talk is an undesirable phenomenon that occurs when a particle is detected in one detector, and then by any means (*e.g.* elastic scattering), the same particle is detected in a different detector. If both detections occur within the time frame typical for neutrons, then the cross-talk event cannot be distinguished

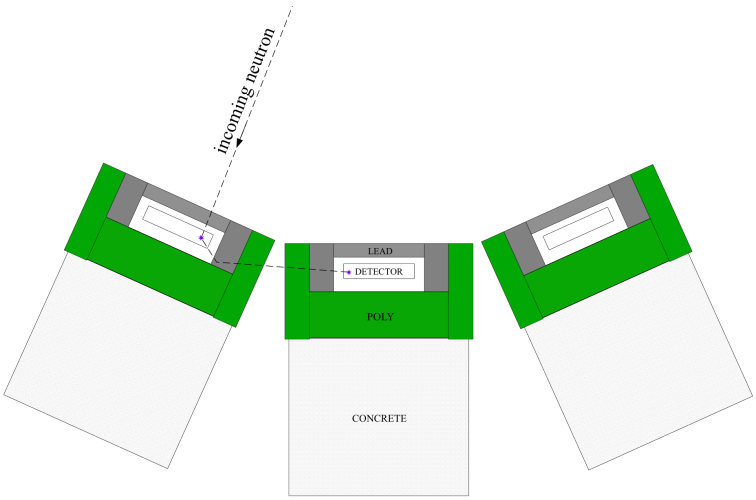

Figure 4.3: A hypothetical example of a neutron cross-talk event. First, an incoming neutron enters a detector and is detected as the result of a collision with a proton. Next, it scatters from some lead shielding nearby, which changes its direction of travel such that it enters a second detector where it is detected a second time. The scattering of a neutron from an intermediate nucleus, in this case a lead nucleus in the detector's shielding, is kinematically required in order for cross-talk to occur in this experiment.

from a true neutron coincidence. The geometry of the neutron detector array makes it kinematically impossible for a neutron to scatter from a proton in one detector–which is the basis for scintillation–and then travel directly to another detector with enough kenetic energy to be detected. Rather, in order for cross-talk to occur, it is required that the neutron scatter from at least one intermediate nucleus while traveling between detectors. This fact, which can be derived from the conservation of energy and momentum, makes cross-talk a "second-order" effect, because upon depositing enough energy to be detected in one detector, the neutron must then 1) scatter from an intermediate nucleus, and 2) be detected in a second detector. However, the fact that cross-talk is a second-order effect is not sufficient to make the claim that cross-talk is negligible, because the detectors and their shielding contain significant levels of carbon, lead, and other nuclei which can function as intermediate scattering points.

ToDo: include the other plot once the god dam wiki is back up.

To address this, a detailed MCNP-PoliMi [11] simulation was performed that includes the entire array of neutron detectors, along with their shielding, supporting structures, and the concrete composing the experimental cell which contains the detectors. PoliMi is an extension to MCNP that was developed to simulate correlated fission particles and their subsequent interactions as accurately as possible. PoliMi includes multiplicity distributions for neutrons, photons, and the correct correlated photon production from neutron interactions. These features are in contrast to the standard release of MCNP which uses uncorrelated distributions and average multiplicities. As a result, the standard release of MCNP converges to the correct average result quicker than if correlated event-by-event distributions were used. Another feature PoliMi provides is the ability for particle tracking data to be printed and post processed by the user. Here, the particle tracking data is used to model detector physics in order to estimate the ratio of the rate of cross-talk to the rate of the detection of correlated neutrons. Neutron detection physics was modeled by converting the amount of energy deposited by neutrons into scintillation light output, and did not include the propagation or detection of scintillation light. The scintillation light output is given in MeV equivalent electron energy, denoted MeVee. Neutron energy deposited from collisions with hydrogen and carbon nuclei is the only input used to calculate light output, the procedures of which are taken from ref [8]. For neutron collisions with hydrogen, the light output in MeVee, L, is given by the following empirical relationship

$$L = 0.0364E_n^2 + 0.125E_n$$

where E_n is equal to the change in the kinetic energy of the neutron during the collision. Neutron interactions with carbon are assumed to generate a smaller

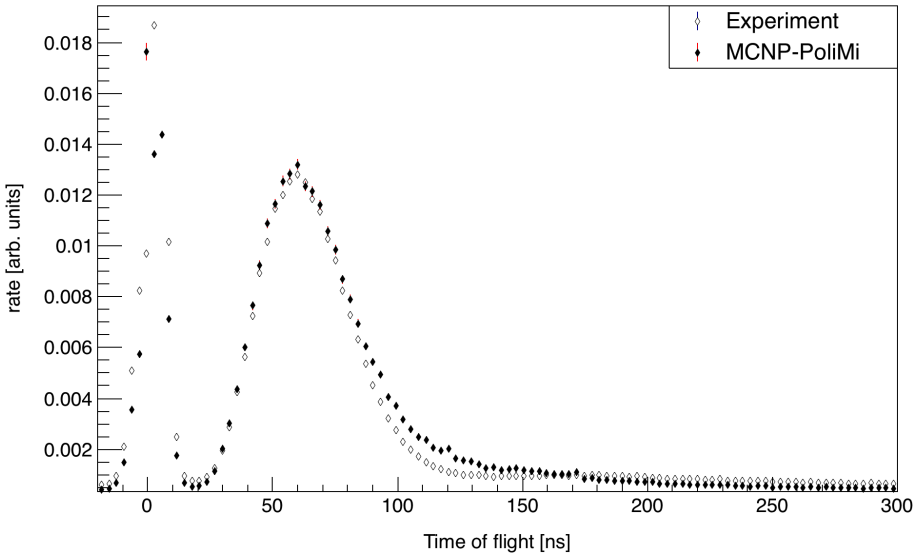

Figure 4.4: Measured vs simulated ToF spectrum of a ^{252}Cf spontaneous fission source. In the simulation, the light output threshold for detection was varied until the result was in good agreement with measurement.

light output of

$$L = 0.02E_n$$

The simulation used MCNP-PoliMi's built in ^{252}Cf spontaneous fission source, which emits neutrons with the correct correlations. The light output threshold for detection was set empirically by choosing the threshold that gave the best agreement between the ToF spectra of simulation and measurement (see fig 4.4). A tally is kept of the number of cross-talk events and the number of correlated neutron pairs detected. An event is considered a "neutron event" if there is a light output of greater than 0.03 MeVee produced in a detector in a time frame of 10 ns or less. Furthermore, the 0.03 MeVee light output threshold must be reached sometime during the neutron time of flight window used in the experiment, which is 45 to 150 ns. This way, the method used for particle identification in the simulation mimics that which is used in the experiment. The opening angle is calculated from the positions at which

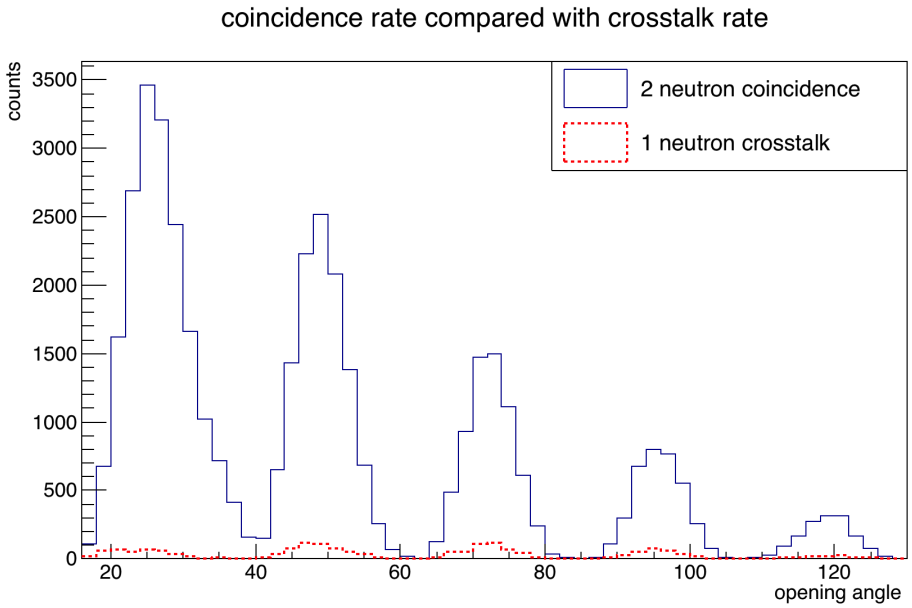

Figure 4.5: Number of cross-talk events and two-neutron coincidences as a function of opening angle.

each particle produced a light output above the 0.03 MeVee threshold. In the simulation, cross-talk events accounted for 3% of total coincident events. Accordingly, no cross-talk corrections were applied to the data. Figure 4.5 shows the distribution of cross-talk events as a function of opening angle.

4.2.2 Elastic Scattering in Target

One consideration for the design of the target was the probability that fission neutrons produced in the target will scatter before exiting the target. This is a cause for concern, because the scattering of neutrons from heavy nuclei highly alters the neutron's direction of travel, creating two-neutron opening angles that are not reflective of the true opening angle immediately after fission. This effect cannot be completely eliminated, but the target must be small enough such that neutron scattering is negligible. The size of such target was found by performing an MCNP simulation in which neutrons with an energy spectrum typical of fission neutrons are sampled uniformly within the target. From the

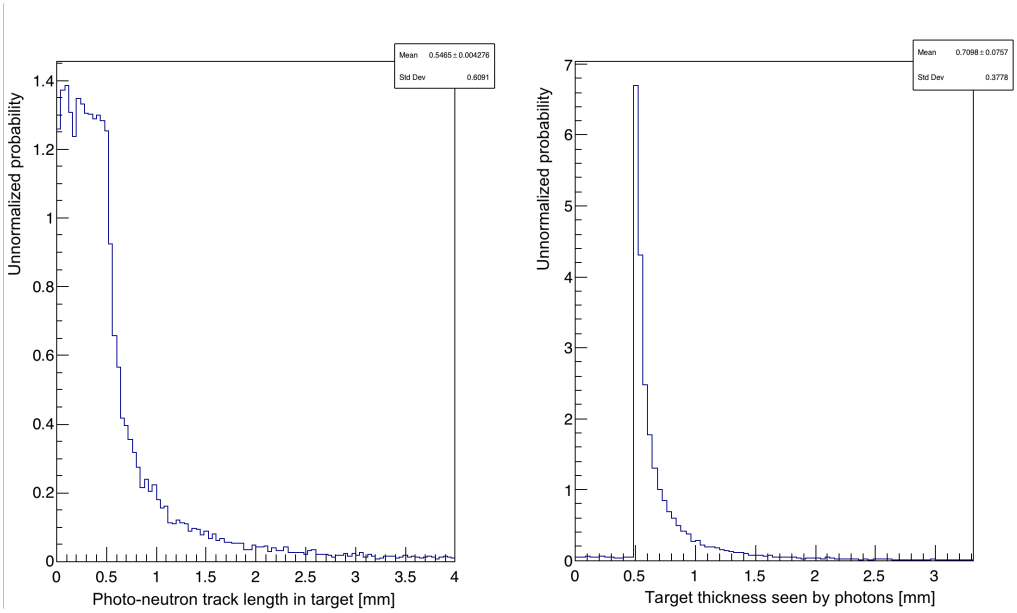

Figure 4.6: Somehow relevant plot.

simulation, 97.5% of the neutrons produced in a DU target with dimensions of 4x2x0.05 cm^3 escaped without scattering. Two neutrons are required for the formation of an opening angle, so the rate of data contamination due to scattering is $(1 - .975^2)$, or 5% of two-neutron events.

ToDo: Maybe expand on this section a little bit. Add the plot of contamination VS radius for Th. Do simulation for DU

Chapter 5

Concluding Remarks

In summary, we have reported on the first ever measurement of two-neutron opening angle distributions from the photofission of ^{238}U, and their dependence on mean neutron energy. Photofission was achieved by means of a Bremsstrahlung photon beam produced by the passage of 10.5 MeV electrons through a 1" thick slab of Aluminum. Electrons were produced by a 44 MeV capable, low duty factor, pulsed linear accelerator housed at the Idaho Accelerator Center.

By virtue of performing a measurement of pairs of correlated fission neutrons, an equivalent distribution of uncorrelated neutron pairs was able be constructed, which served as a normalizing distribution. By normalizing measurements to this distribution, the dependence of the measurement on detector efficiencies and geometry is eliminated.

Appendix A

Dummy Appendix

ToDo: put some MCNP decks here, just because.

Bibliography

[1] Harry R. Bowman, Stanley G. Thompson, J. C. D. Milton, and Wladyslaw J. Swiatecki. Velocity and angular distributions of prompt neutrons from spontaneous fission of cf^{252}. *Phys. Rev.*, 126:2120–2136, Jun 1962.

[2] C. Budtz-JÃžrgensen and H.-H. Knitter. Simultaneous investigation of fission fragments and neutrons in 252cf (sf). *Nuclear Physics A*, 490(2):307 – 328, 1988.

[3] J. T. Caldwell, E. J. Dowdy, R. A. Alvarez, B. L. Berman, and P. Meyer. Experimental determination of photofission neutron multiplicities for 235u, 236u, 238u, and 232th using monoenergetic photons. *Nuclear Science and Engineering*, 73(2):153–163, 1980.

[4] S. Debenedetti, J. E. Francis, W. M. Preston, and T. W. Bonner. Angular dependence of coincidences between fission neutrons. *Phys. Rev.*, 74:1645–1650, Dec 1948.

[5] A. M. Gagarski, I. S. Guseva, V. E. Sokolov, G. V. Val'Ski, G. A. Petrov, D. O. Krinitsin, D. V. Nikolaev, T. A. Zavarukhina, and V. I. Petrova. Neutron-neutron angular correlations in spontaneous fission of 252Cf. *Bulletin of the Russian Academy of Sciences, Physics*, 72:773–777, July 2008.

[6] HAMAMATSU PHOTONICS. *PHOTOMULTlPLlER TUBE R580*, 1 1999.

[7] N.V Kornilov, A.B Kagalenko, S.V Poupko, P.A Androsenko, and F.-J Hambsch. New evidence of an intense scission neutron source in the 252cf spontaneous fission. *Nuclear Physics A*, 686(1):187 – 203, 2001.

[8] Eric C. Miller, Shaun D. Clarke, Marek Flaska, Sara A. Pozzi, and Enrico Padovani. Mcnpx-polimi post-processing algorithm for detector response simulations. *JNMM, Journal of the Institute of Nuclear Materials Management*, 40(2):34–41, 12 2012.

[9] S Nair, D B Gayther, B H Patrick, and E M Bowey. Fission-neutron and fragment angular distributions from threshold photofission of 232 th and 238 u. *Journal of Physics G: Nuclear Physics*, 3(7):965, 1977.

[10] G. A. Petrov. Current status of the search for scission neutrons in fission and estimation of their main characteristics. *AIP Conference Proceedings*, 798(1):205–212, 2005.

[11] Sara A Pozzi, Enrico Padovani, and Marzio Marseguerra. Mcnp-polimi: a monte-carlo code for correlation measurements. *Nuclear Instruments and Methods in Physics Research Section A: Accelerators, Spectrometers, Detectors and Associated Equipment*, 513(3):550 – 558, 2003.

[12] Sara A. Pozzi, Brian Wieger, Andreas Enqvist, Shaun D. Clarke, Marek Flaska, Matthew Marcath, Edward Larsen, Robert C. Haight, and Enrico Padovani. Correlated neutron emissions from 252cf. *Nuclear Science and Engineering*, 178(2):250–260, 2014.

[13] J. S. Pringle and F. D. Brooks. Angular correlation of neutrons from spontaneous fission of ^{252}Cf. *Phys. Rev. Lett.*, 35:1563–1566, Dec 1975.

[14] C. P. Sargent, W. Bertozzi, P. T. Demos, J. L. Matthews, and W. Turchinetz. Prompt neutrons from thorium photofission. *Phys. Rev.*, 137:B89–B101, Jan 1965.

[15] Seregina. *Measurements and Analysis of Angular-Energy Distribution for 252Cf (SF) neutrons*. PhD thesis, IPPE, Obninsk, Russia, 1985.

[16] Olivier Serot, Olivier Litaize, and Abdelaziz Chebboubi. Influence of scission neutrons on the prompt fission neutron spectrum calculations. In *EPJ Web of Conferences*, volume 146, page 04027. EDP Sciences, 2017.

[17] V. E. Sokolov and G. A. Petrov. Investigation of the angular dependences of neutron-neutron coincidences from 252cf, 235u, 233u and 239pu fission in search of scission neutrons. *Proc. XVIII Internat. Seminar on Interaction of Neutrons with Nuclei (ISSIN-18)*, pages 108–118, 2010.